IEEE Access
Multidisciplinary ⋮ Rapid Review ⋮ Open Access Journal

Received December 22, 2018, accepted January 24, 2019, date of publication February 19, 2019, date of current version March 4, 2019.

Digital Object Identifier 10.1109/ACCESS.2019.2898703

An Analytical Decoupled Corner Smoothing Method for Five-Axis Linear Tool Paths

XIN ZHAO[1], HUAN ZHAO[1], SHAOHUA WAN[1,2], (Member, IEEE), XIANGFEI LI[1], AND HAN DING[1]

[1]State Key Laboratory of Digital Manufacturing Equipment and Technology, Huazhong University of Science and Technology, Wuhan 430074, China
[2]School of Information and Safety Engineering, Zhongnan University of Economics and Law, Wuhan 430073, China

Corresponding author: Huan Zhao (huanzhao@hust.edu.cn)

This work was supported in part by the National Key Research and Development Program of China under Grant 2017YFB1303401, and in part by the National Natural Science Foundation of China under Grant 91748114, Grant 51535004, and Grant 51705175.

ABSTRACT Nowadays, the tool path in five-axis machining is usually described with linear segments. Tangential and curvature discontinuities of the linear tool path lead to poor machining efficiency and quality. Due to the complexities in constraining approximation errors and synchronization of tool tip position and tool orientation, it still remains a challenge to smooth five-axis linear tool path in real-time. To solve this problem, this paper developed an analytical decoupled corner smoothing method by inserting an asymmetric cubic B-spline and a pair of symmetric quartic spherical Bézier curves for tool tip position and tool orientation, respectively. The maximal approximation errors for tool tip position and tool orientation are fully constrained in the blending procedures. Tool tip position and tool orientation are synchronized by adjusting the blending lengths and angles, which guarantees the C^2 continuity of the tool path. The blending and synchronous scheme are analytical. Therefore, the proposed method can be employed in real-time. To verify the proposed method, simulations and experiments on a five-axis machine tool are conducted, the results demonstrate the feasibility and efficiency of the proposed method.

INDEX TERMS Corner smoothing, five-axis, spherical Bézier, CNC, B-spline.

I. INTRODUCTION

Five-axis CNC machining is widely used to machine workpieces with complex shapes, such as impellers, turbine blades and aerospace structure parts. Nowadays, linear tool paths are still the most common format of tool path in CNC machining. Due to the tangential and curvature discontinuities of linear tool paths, fluctuation of feedrate and acceleration may lead to vibration of machine tool and long machining time. To improve the machining efficiency and quality, tool path smoothing methods are usually adopted [1]–[4].

There are two major kinds of tool path smoothing methods, i.e. global smoothing method and local smoothing method. Global smoothing method utilizes splines to interpolate or approximate the linear tool path. Langeron *et al.* [5] utilized two B-Spline to synchronously interpolate the positions of tool tip and a point on the tool axis. Based on this idea, Wang *et al.* [6] realized a double NURBS curve based interpolator and integrated it to an open CNC system. Zhang *et al.* [7] generated smooth tool path using rational Bézier motions for five-axis sculptured surface machining. Bi *et al.* [8] extended this idea, and proposed a dual quaternion based algorithm to generate compact dual NURBS tool path with equal distance. After that, Zhao *et al.* [9] proposed an approximation method using dual quaternion with dominant point. In [5]–[9], tool tip position and tool orientation are coupled. In contrast to the coupled method, Fleisig and Spence [10] proposed a triple-spline based interpolation method: a near arc-length quintic polynomial position spline interpolates the tool tip positions, a quintic spherical Bézier spline interpolates the tool orientation vectors, and a quadratic spline is utilized to reparametrize the two previous splines. Yuen *et al.* [11] developed a jerk-continuous interpolation method, which fits the tool tip positions and orientations to quintic splines independently, then utilizes ninth order and seventh order feed correction splines to approximate the nonlinear relationship between spline parameters and displacements along the path for tool tip positions and tool orientations respectively. Later, Yang and Altintas [12] improved this method by transforming tool orientation vectors into quaternion space to solve the singular problem. However, for the global smoothing method,

The associate editor coordinating the review of this manuscript and approving it for publication was Bora Onat.

it is still challenging to control the approximation errors between two adjacent input points, especially for five-axis tool path.

Unlike the global smoothing method, the local smoothing method blends corner with splines but remains part of linear segments. Local smoothing method has been widely studied in tri-axis machining [13]–[16]. Yang and Sukkarieh [13] smoothed corner with a pair of cubic Bézier curves satisfying both curvature continuity and maximum curvature requirements simultaneously. Zhao *et al.* [14] adopted a curvature-continuous cubic B-spline to blend the linear segments. Fan *et al.* [15] proposed a real-time local smoothing method, which generates G^3 interpolative tool path with quartic Bézier curves. Duan and Okwudire [16] used an optimal control method to generate the best free-form curve that minimizes machining time under the constraints of path tolerance and kinematics.

For five-axis tool paths, local smoothing procedure can be employed in machine tool coordinate system (MCS) or part coordinate system (PCS). Beudaert *et al.* [17] proposed an iterative method to increase the real feedrate by smoothing the joint motions. Bi *et al.* [18] proposed an analytical curvature-continuous dual-Bézier corner transition method in MCS, which utilizes one cubic Bézier curve to smooth the translational path, and another for the rotational path. However, this kind of methods is related to the configuration of machine tool. Beudaert *et al.* [19] utilized two cubic B-splines to blend the corner of tool tip position and a reference point on tool axis, meanwhile, a third spline was constructed to optimize the orientation connection with tool tip position. Jin *et al.* [20] proposed a dual-Bézier based method, and Shi *et al.* [21] blended corner with a pair of PH curves. Different from the coupled methods [19]–[21], Tulsyan *et al.* [22] proposed a decoupled method, which uses a quintic B-spline to blend tool tip position and a near-unit B-spline for tool orientation respectively. The control points are optimized to achieve C^3 continuity at the junctions while respecting pre-given tolerance. However, due to the optimization in the calculation of control points, this method is hard to be employed in real-time. Yang and Yue [23] smoothed the tool tip position in PCS and the tool orientation in MCS, respectively. The tool orientation smoothing error was indirectly constrained with forward kinematics.

In this paper, an analytical decoupled local smoothing method for five-axis linear tool paths is proposed. The tool tip position is smoothed with an asymmetric cubic B-spline, and the tool orientation is smoothed with a pair of symmetric quartic spherical Bézier within the given tolerances, which guarantees unit property of tool orientation vector. In this method, the approximation error bounds for both tool tip position and tool orientation are analytical. Meanwhile, a synchronous scheme is used to synchronize tool tip position and tool orientation and achieve C^2 continuity simultaneously. Because all the calculations are analytical, the proposed method can be employed in real-time.

The remainder of this paper is organized as follows. In Section 2, the asymmetric cubic B-spline based transition scheme for tool tip position is introduced. In Section 3, the principle of spherical Bézier curve is provided, and then, the tool orientation transition scheme is introduced. The details of the local smoothing procedure are described in Section 4. In Section 5, simulation and experimental validations are presented. The conclusions are given in Section 6.

II. TOOL TIP POSITION SMOOTHING

A linear five-axis path is represented by tool tip positions $\mathbf{p}_i = [x_i,\ y_i,\ z_i]$ and tool orientation vectors $\mathbf{o}_i = [i_i,\ j_i,\ k_i]$, where $i \in [0,\ n]$ is the index of the discrete points, and $\mathbf{o}_i$ are unit vectors, i.e. $i_i^2 + j_i^2 + k_i^2 = 1$. In the proposed method, sharp corner is blended with an asymmetric cubic B-spline for tool tip position and a pair of symmetric quartic spherical Bézier curves for tool orientation vector. In our previous work [14], a cubic B-spline based transition scheme for three-axis tool path is introduced, the blending lengths in two neighboring linear segments are equal. However, in this proposed method, the blending lengths are adjusted unequally to synchronize tool tip position and tool orientation.

A. PRELIMINARY OF CUBIC B-SPLINE

The cubic B-spline is utilized to blend the linear segments of tool tip position, which is defined as [24]

$$\mathbf{C}(u) = \sum_{i=0}^{n} N_{i,3}(u)\,\mathbf{Q}_i, \quad u \in [0,\ 1], \tag{1}$$

where $\mathbf{Q}_i$ are the control points, $N_{i,3}(u)$ is the i-th cubic B-spline basis function, which is defined as

$$N_{i,0}(u) = \begin{cases} 0, & u_i \le u \le u_{i+1} \\ 1, & otherwise \end{cases},$$
$$N_{i,k}(u) = \frac{u - u_i}{u_{i+k} - u_i} N_{i,k-1}(u) + \frac{u_{i+k+1} - u}{u_{i+k+1} - u_{i+1}} N_{i+i,k-1}(u), \tag{2}$$

where $\mathbf{U} = [u_0,\ u_1,\ \ldots,\ u_m]$ is the knot vector.

B. TRANSITION SCHEME FOR TOOL TIP POSITION

As shown in Fig.1, a cubic B-spline $\mathbf{C}(u)$ is constructed to blend the tool tip position corner defined by two

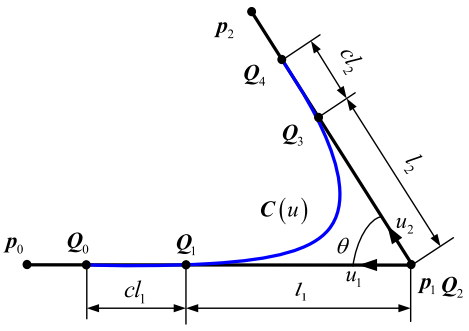

FIGURE 1. The transition cubic B-spline of the neighboring tool tip positions.

linear segments $\mathbf{p}_0\mathbf{p}_1$ and $\mathbf{p}_1\mathbf{p}_2$. To achieve tangential and acceleration continuities at the junctions $\mathbf{Q}_0\,(u=0)$ and $\mathbf{Q}_4\,(u=1)$, the knot vector is constructed as $\mathbf{U} = [0,\ 0,\ 0,\ 0,\ 0.5,\ 1,\ 1,\ 1,\ 1]$, the first two control points $\mathbf{Q}_0$ and $\mathbf{Q}_1$ are located in the linear segment $\mathbf{p}_0\mathbf{p}_1$, the last two points $\mathbf{Q}_3$ and $\mathbf{Q}_4$ are located in the linear segment $\mathbf{p}_1\mathbf{p}_2$ meanwhile, the third control point $\mathbf{Q}_2$ coincides with $\mathbf{p}_1$.

The second derivatives of the cubic B-spline with respect to arc length s at two junctions are

$$\begin{aligned}\left.\frac{\mathrm{d}^2\mathbf{C}\,(u)}{\mathrm{d}s^2}\right|_{u=0} &= \frac{\mathrm{d}^2\mathbf{C}\,(u)}{\mathrm{d}u^2}\left(\frac{\mathrm{d}u}{\mathrm{d}s}\right)^2 + \frac{\mathrm{d}\mathbf{C}\,(u)}{\mathrm{d}u}\left.\frac{\mathrm{d}^2u}{\mathrm{d}s^2}\right|_{u=0},\\ \left.\frac{\mathrm{d}^2\mathbf{C}\,(u)}{\mathrm{d}s^2}\right|_{u=1} &= \frac{\mathrm{d}^2\mathbf{C}\,(u)}{\mathrm{d}u^2}\left(\frac{\mathrm{d}u}{\mathrm{d}s}\right)^2 + \frac{\mathrm{d}\mathbf{C}\,(u)}{\mathrm{d}u}\left.\frac{\mathrm{d}^2u}{\mathrm{d}s^2}\right|_{u=1},\end{aligned} \tag{3}$$

where

$$\begin{aligned}\left.\frac{\mathrm{d}\mathbf{C}\,(u)}{\mathrm{d}u}\right|_{u=0} &= 6cl_1\mathbf{u}_1, \quad \left.\frac{\mathrm{d}^2\mathbf{C}\,(u)}{\mathrm{d}u^2}\right|_{u=0} = 12\,(1-2c)\,l_1\mathbf{u}_1,\\ \left.\frac{\mathrm{d}\mathbf{C}\,(u)}{\mathrm{d}u}\right|_{u=1} &= 6cl_2\mathbf{u}_2, \quad \left.\frac{\mathrm{d}^2\mathbf{C}\,(u)}{\mathrm{d}u^2}\right|_{u=1} = 12\,(2c-1)\,l_2\mathbf{u}_2,\\ \left.\frac{\mathrm{d}u}{\mathrm{d}s}\right|_{u=0} &= \frac{1}{6cl_1}, \quad \left.\frac{\mathrm{d}^2u}{\mathrm{d}s^2}\right|_{u=0} = \frac{2c-1}{18c^3l_1^2},\\ \left.\frac{\mathrm{d}u}{\mathrm{d}s}\right|_{u=1} &= \frac{1}{6cl_2}, \quad \left.\frac{\mathrm{d}^2u}{\mathrm{d}s^2}\right|_{u=1} = \frac{1-2c}{18c^3l_2^2},\end{aligned} \tag{4}$$

where l_1 and l_2 are the blending lengths, $\mathbf{u}_1$ and $\mathbf{u}_2$ are the unit vectors along $\mathbf{p}_1\mathbf{p}_0$ and $\mathbf{p}_1\mathbf{p}_2$ respectively, as shown in Fig. 1. By setting $c = 0.5$, the second derivatives in Eq.(4) equal zero, which guarantees the G^2 continuity, meanwhile simplifies the calculation of tool orientation transition.

The approximation error bound is

$$\varepsilon_b = \frac{l}{2}\cos\frac{\theta}{2}, \tag{5}$$

where $l = \max(l_1, l_2)$, and θ is the angle between $\mathbf{u}_1$ and $\mathbf{u}_2$.The proof is provided in Appendix A. To ensure the approximation accuracy, the blending lengths must be constrained.

As shown in Fig. 1, the blended lengths are $|\mathbf{Q}_0\mathbf{Q}_2| = 3l_1/2$ and $|\mathbf{Q}_2\mathbf{Q}_4| = 3l_2/2$ respectively. Because each linear segment except the two end ones is blended by two corners, the maximum blending length can be consequently defined by

$$l \le \min\left\{2\varepsilon_{tip}\sec\frac{\theta}{2}, \frac{L_1}{3}, \frac{L_2}{3}\right\}, \tag{6}$$

where ε_{tip} is the specified tolerance of the tool tip position, L_1 and L_2 are the lengths of $\mathbf{p}_1\mathbf{p}_0$ and $\mathbf{p}_1\mathbf{p}_2$ respectively.

III. TOOL ORIENTATION SMOOTHING

A. PRELIMINARY OF SPHERICAL BÉZIER CURVE

The spherical Bézier curve constructed with the de Castljau form lies on the unit sphere, which is suitable for describing the tool orientation vector [9]. The spherical Bézier curve of degree j is defined as

$$\mathbf{B}_k^j(v) = \begin{cases}\mathbf{B}_k, & j=0\\ \dfrac{\mathbf{B}_k^{j-1}(v)\sin[\theta(1-v)] + \mathbf{B}_{k+1}^{j-1}\sin(\theta v)}{\sin\theta}, & j>0\end{cases} \tag{7}$$

where the three dimensional vectors $\mathbf{B}_k$ satisfying $|\mathbf{B}_k| = 1$ are the control points, $v \in [0,\ 1]$ is the parameter, and $\theta = \arccos\left[\mathbf{B}_k^{j-1}(v)\cdot\mathbf{B}_{k+1}^{j-1}(v)\right]$ is the angle between $\mathbf{B}_k^{j-1}(v)$ and $\mathbf{B}_{k+1}^{j-1}(v)$.

The first and second derivatives for the quartic spherical Bézier curve at two end points are provided in Appendix B. It can be found that, the curve passes through the first and last control points, the first derivatives at two end points of a segment depend only on the first and last two control points, and the second derivatives depend only on the first and last three control points. With these benefits, two symmetric quartic spherical Bézier curves are utilized to blend the tool orientation corner.

B. TRANSITION SCHEME FOR TOOL ORIENTATION

A corner of tool orientation is shown in Fig. 2, two symmetric quartic spherical Bézier curves $\mathbf{B}_1(v)$ and $\mathbf{B}_2(v)$ are constructed to blend the corner. To simplify the calculation, the control points $\mathbf{B}_0$, $\mathbf{B}_1$, and $\mathbf{B}_2$ lie on a great circle of the unit sphere, $\mathbf{B}_2, \ldots, \mathbf{B}_6$ and $\mathbf{B}_6$, $\mathbf{B}_7$, $\mathbf{B}_8$ are similar. θ_i is the angle between $\mathbf{B}_i$ and $\mathbf{B}_{i+1}$ on the great circle. β_1 and β_2 are the angles between $\mathbf{o}_1$ and $\mathbf{B}_2$, $\mathbf{B}_6$ respectively.

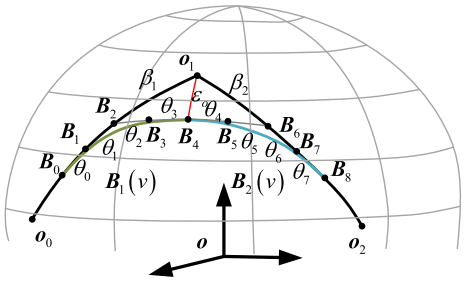

FIGURE 2. The transition scheme for tool orientation.

Furthermore, $\mathbf{B}_1(v)$ and $\mathbf{B}_2(v)$ are constructed symmetrically, i.e. $\theta_0 = \theta_7$, $\theta_1 = \theta_6$, $\theta_2 = \theta_5$, $\theta_3 = \theta_4$ and $\beta_1 = \beta_2 = \beta$. Because tool tip position is blended by one B-spline, while tool orientation is blended by two curves, the mapping between the parameter v of $\mathbf{B}_1(v)$, $\mathbf{B}_2(v)$ and the parameter u of the tool tip position blended curve $\mathbf{C}(u)$ must be defined. To simplified the calculation, the mappings are defined as $v = 2u$, $(u \in [0,\ 0.5])$ for $\mathbf{B}_1(v)$, $v = 2\,(u-0.5)$, $(u \in [0.5,\ 1])$ for $\mathbf{B}_2(v)$.

The linear segments $\widehat{\mathbf{o}_0\mathbf{o}_1}$ and $\widehat{\mathbf{o}_1\mathbf{o}_2}$ are represented with linear spherical curves [25]

$$\begin{aligned}\mathbf{o}_1(u) &= \frac{\mathbf{o}_0\sin[\phi\,(1-u)] + \mathbf{o}_1\sin(u\phi)}{\sin\phi}\\ \mathbf{o}_2(u) &= \frac{\mathbf{o}_1\sin[\psi\,(1-u)] + \mathbf{o}_2\sin(u\psi)}{\sin\psi}\end{aligned} \tag{8}$$

where $u \in [0,\ 1]$ is the parameter, $\phi = \arccos \mathbf{o}_0\mathbf{o}_1$ and $\psi = \arccos \mathbf{o}_1\mathbf{o}_2$ are the angles for $\widehat{\mathbf{o}_0\mathbf{o}_1}$ and $\widehat{\mathbf{o}_1\mathbf{o}_2}$ respectively.

Note that, the tool tip position linear segment $\mathbf{p}_0\mathbf{p}_1$ is $\mathbf{p}(u) = (1-u)\mathbf{p}_0 + u\mathbf{p}_1$, $u \in [0, 1]$. To synchronize the tool tip position and tool orientation, the the tool tip position junction point $\mathbf{Q}_0$ and tool orientation junction point $\mathbf{B}_0$ should have the same parameter u, which means the ratio of the blended angle $\angle\mathbf{B}_0\mathbf{o}\mathbf{o}_1 / \angle\mathbf{o}_1\mathbf{o}\mathbf{B}_8$ to the total angle ϕ/ψ should equal to the ratio of the blended length $|\mathbf{Q}_0\mathbf{p}_1| / |\mathbf{p}_1\mathbf{Q}_4|$ to the total path length L_1/L_2, i.e. the following relationship should be satisfied:

$$\begin{aligned} \frac{\theta_0 + \theta_1 + \beta}{\phi} &= \frac{(1+c)\, l_1}{L_1} = \frac{3l_1}{2L_1}, \\ \frac{\theta_6 + \theta_7 + \beta}{\psi} &= \frac{(1+c)\, l_2}{L_2} = \frac{3l_2}{2L_2}. \end{aligned} \tag{9}$$

As mentioned in [19], in order to achieve feedrate and acceleration continuities at the junction points $\mathbf{B}_0$, $\mathbf{B}_4$ and $\mathbf{B}_8$, the following relationships must be satisfied:

$$\begin{aligned} \left.\frac{\mathrm{d}\mathbf{o}_1(u)}{\mathrm{d}s}\right|_{\mathbf{B}_0} &= \left.\frac{\mathrm{d}\mathbf{B}_1(v)}{\mathrm{d}s}\right|_{u=0}, \\ \left.\frac{\mathrm{d}^2\mathbf{o}_1(u)}{\mathrm{d}s^2}\right|_{\mathbf{B}_0} &= \left.\frac{\mathrm{d}^2\mathbf{B}_1(v)}{\mathrm{d}s^2}\right|_{u=0}, \\ \left.\frac{\mathrm{d}\mathbf{o}_2(u)}{\mathrm{d}s}\right|_{\mathbf{B}_8} &= \left.\frac{\mathrm{d}\mathbf{B}_2(v)}{\mathrm{d}s}\right|_{u=1}, \\ \left.\frac{\mathrm{d}^2\mathbf{o}_2(u)}{\mathrm{d}s^2}\right|_{\mathbf{B}_8} &= \left.\frac{\mathrm{d}^2\mathbf{B}_2(v)}{\mathrm{d}s^2}\right|_{u=1}, \\ \left.\frac{\mathrm{d}\mathbf{B}_1(v)}{\mathrm{d}s}\right|_{v=1} &= \left.\frac{\mathrm{d}\mathbf{B}_2(v)}{\mathrm{d}s}\right|_{v=0}, \\ \left.\frac{\mathrm{d}^2\mathbf{B}_1(v)}{\mathrm{d}s^2}\right|_{v=1} &= \left.\frac{\mathrm{d}^2\mathbf{B}_2(v)}{\mathrm{d}s^2}\right|_{v=0}. \end{aligned} \tag{10}$$

These relationships can be ensured with **Theorem 1** and **Theorem 2**.

Theorem 1: As shown in Fig. 2, if $\theta_0 = \theta_1 = 3l_1\phi/8L_1$ holds, then $\mathbf{o}_1(u)$ and $\mathbf{B}_1(v)$ is C^2 continuous with respect to tool tip position length parameter s at $\mathbf{B}_0$.

Proof: The first and second derivatives of $\mathbf{o}_1(u)$ with respect to tool tip position length s at the junction point $\mathbf{B}_0$ are

$$\begin{aligned} \left.\frac{\mathrm{d}\mathbf{o}_1(u)}{\mathrm{d}s}\right|_{\mathbf{B}_0} &= \frac{\phi}{L_1 \sin\phi}\left[\mathbf{o}_1 \cos(\phi - \beta - \theta_0 - \theta_1)\right. \\ &\quad \left. - \mathbf{o}_0 \cos(\beta + \theta_0 + \theta_1)\right], \\ \left.\frac{\mathrm{d}^2\mathbf{o}_1(u)}{\mathrm{d}s^2}\right|_{\mathbf{B}_0} &= -\frac{\phi^2}{{L_1}^2 \sin\phi}\left[\mathbf{o}_1 \sin(\phi - \beta - \theta_0 - \theta_1)\right. \\ &\quad \left. + \mathbf{o}_0 \sin(\beta + \theta_0 + \theta_1)\right]. \end{aligned} \tag{11}$$

With Eqs.(4), (27) and (28), the first and second derivatives of $\mathbf{B}_1(v)$ at the junction point $\mathbf{B}_0$ are

$$\begin{aligned} \left.\frac{\mathrm{d}\mathbf{B}_1(v)}{\mathrm{d}s}\right|_{u=0} &= \left.\frac{\mathrm{d}\mathbf{B}_1(v)}{\mathrm{d}v}\frac{\mathrm{d}v}{\mathrm{d}u}\frac{\mathrm{d}u}{\mathrm{d}s}\right|_{u=0} \\ &= \frac{8\theta_0}{3l_1 \sin\phi}\left[-\mathbf{o}_0 \cos(\beta + \theta_0 + \theta_1)\right. \\ &\quad \left. + \mathbf{o}_1 \cos(\beta + \theta_0 + \theta_1 - \phi)\right], \\ \left.\frac{\mathrm{d}^2\mathbf{B}_1(v)}{\mathrm{d}s^2}\right|_{u=0} &= \left.\left(\frac{\mathrm{d}^2\mathbf{B}_1(v)}{\mathrm{d}v^2}\frac{\mathrm{d}v}{\mathrm{d}u}\frac{\mathrm{d}u}{\mathrm{d}s} + \frac{\mathrm{d}\mathbf{B}_1(v)}{\mathrm{d}v}\frac{\mathrm{d}v}{\mathrm{d}u}\frac{\mathrm{d}^2u}{\mathrm{d}s^2}\right)\right|_{u=0} \\ &= -\frac{\mathbf{o}_0}{9l_1^2 \sin\phi}\left[-48(\theta_0 - \theta_1)\cos(\beta + \theta_0 + \theta_1)\right. \\ &\quad \left. + 64{\theta_0}^2 \sin(\beta + \theta_0 + \theta_1)\right] \\ &\quad + \frac{\mathbf{o}_1}{9l_1^2 \sin\phi}\left[64{\theta_0}^2 \sin(\beta + \theta_0 + \theta_1 - \phi)\right. \\ &\quad \left. - 48(\theta_0 - \theta_1)\cos(\beta + \theta_0 + \theta_1 - \phi)\right]. \end{aligned} \tag{12}$$

It can be found that, if the following relation holds, Eq. (10) is satisfied, i.e. $\mathbf{o}_1(u)$ and $\mathbf{B}_1(v)$ is C^2 continuous at $\mathbf{B}_0$.

$$\theta_0 = \theta_1 = \frac{3l_1\phi}{8L_1}. \tag{13}$$

Similarly, we can also prove that, if $\theta_6 = \theta_7 = 3l_2\psi/8L_2$ holds, $\mathbf{o}_2(u)$ and $\mathbf{B}_2(v)$ are C^2 continuous with respect to tool tip position length s at $\mathbf{B}_8$.

Except two end junctions, $\mathbf{B}_1(v)$ and $\mathbf{B}_2(v)$ should be C^2 continuous at $\mathbf{B}_4$ too, which can be guaranteed by **Theorem 2**.

Theorem 2: If $\theta_2 = \theta_3 = \theta_4 = \theta_5$ holds, $\mathbf{B}_1(v)$ and $\mathbf{B}_2(v)$ are C^2 continuous at $\mathbf{B}_4$.

Proof: Note that, the first and second derivatives $\mathrm{d}v/\mathrm{d}s$ and $\mathrm{d}^2v/\mathrm{d}s^2$ for $\mathbf{B}_1(v)$ and $\mathbf{B}_2(v)$ at $\mathbf{B}_4$ are equal. Therefore, the fifth and sixth equations in Eq. (10) can be rewritten as

$$\begin{aligned} \left.\frac{\mathrm{d}\mathbf{B}_1(v)}{\mathrm{d}v}\right|_{v=1} &= \left.\frac{\mathrm{d}\mathbf{B}_2(v)}{\mathrm{d}v}\right|_{v=0}, \\ \left.\frac{\mathrm{d}^2\mathbf{B}_1(v)}{\mathrm{d}v^2}\right|_{v=1} &= \left.\frac{\mathrm{d}^2\mathbf{B}_2(v)}{\mathrm{d}v^2}\right|_{v=0}. \end{aligned} \tag{14}$$

With Eq. (28), Eq. (14) can be rewritten as

$$\begin{aligned} &\frac{5\theta_3}{\sin\theta_3}(\mathbf{B}_4\cos\theta_3 - \mathbf{B}_3) \\ &= \frac{5\theta_4}{\sin\theta_4}(\mathbf{B}_5 - \mathbf{B}_4\cos\theta_4), \\ &\frac{12\theta_3}{\sin\theta_3}\left[\frac{\theta_3\cos^2\theta_3}{\sin\theta_3}\mathbf{B}_4 - \left(\frac{\theta_3\cos\theta_3}{\sin\theta_3} + \frac{\theta_2\cos\theta_2}{\sin\theta_2}\right)\mathbf{B}_3 + \frac{\theta_2}{\sin\theta_2}\mathbf{B}_2\right] \\ &\quad + 12\frac{(\theta_3 - \theta_2)}{\sin^2\theta_3}\left[\mathbf{B}_4(\cos\theta_3\sin\theta_3 - \theta_3)\right. \\ &\quad \left. - \mathbf{B}_3(\sin\theta_3 - \theta_3\cos\theta_3)\right] - 4\theta_3^2\mathbf{B}_4 = -4\theta_4^2\mathbf{B}_4 \\ &\quad + \frac{12\theta_4}{\sin\theta_4}\left[\frac{\theta_4\cos^2\theta_4}{\sin\theta_4}\mathbf{B}_4 - \left(\frac{\theta_4\cos\theta_4}{\sin\theta_4} + \frac{\theta_5\cos\theta_5}{\sin\theta_5}\right)\mathbf{B}_5\right. \\ &\quad \left. + \frac{\theta_5}{\sin\theta_5}\mathbf{B}_6\right] - \frac{12(\theta_4 - \theta_5)}{\sin^2\theta_4} \\ &\quad \times \left[\mathbf{B}_4(\theta_4 - \sin\theta_4\cos\theta_4) + \mathbf{B}_5(\sin\theta_4 - \theta_4\cos\theta_4)\right]. \end{aligned} \tag{15}$$

Obviously, if $\theta_2 = \theta_3 = \theta_4 = \theta_5$ holds, then Eq. (15) is satisfied, in other words, $\mathbf{B}_1(v)$ and $\mathbf{B}_2(v)$ are C^2 continuous at $\mathbf{B}_4$. □

Because $\mathbf{B}_1(v)$ and $\mathbf{B}_2(v)$ are symmetrical, similarly to the tool tip spline, the maximum orientation approximation error occurs at $\mathbf{B}_4$, which is evaluated as

$$\begin{aligned}\varepsilon_o &= \arccos(\mathbf{o}_1 \cdot \mathbf{B}_4) \\ &= \arccos\left(\cos\beta\sqrt{\frac{2\sin\phi\sin\psi}{2\sin\phi\sin\psi - \sin^2\beta\,[\cos(\phi-\psi) - \mathbf{o}_0\cdot\mathbf{o}_2]}}\right)\end{aligned} \tag{16}$$

It can be seen that, the maximum orientation approximation error only depends on β. For a given orientation error tolerance limit ε_{ori}, β is constrained by

$$\beta \le \arccos\sqrt{\frac{[2\sin\phi\sin\psi - \cos(\phi-\psi) - \mathbf{o}_0\cdot\mathbf{o}_2]\cos^2\varepsilon_{ori}}{2\sin\phi\sin\psi - [\cos(\phi-\psi) - \mathbf{o}_0\cdot\mathbf{o}_2]\cos^2\varepsilon_{ori}}}. \tag{17}$$

With Eqs. (9) and (13) the blended angles in Fig. 2 are $\angle\mathbf{B}_0\mathbf{o}\mathbf{o}_1 = \angle\mathbf{o}_1\mathbf{o}\mathbf{B}_8 = 2\beta$. Similarly to the tool tip position, a linear segment of tool orientation is blended by two corners, thus the blending angle of tool orientation must satisfy the following relation

$$\beta \le \min\left\{\frac{\phi}{4}, \frac{\psi}{4}, \arccos\sqrt{\frac{[2\sin\phi\sin\psi - \cos(\phi-\psi) - \mathbf{o}_0\cdot\mathbf{o}_2]\cos^2\varepsilon_{ori}}{2\sin\phi\sin\psi - [\cos(\phi-\psi) - \mathbf{o}_0\cdot\mathbf{o}_2]\cos^2\varepsilon_{ori}}}\right\} \tag{18}$$

Once β is obtained, the angles θ_i $(i = 0, \ldots, 7)$ can all be calculated, and the control points can be constructed with Fig.2.

IV. REAL-TIME C^2 CONTINUOUS LOCAL SMOOTHING PROCEDURE

In this section, the main steps of the proposed real-time C^2 continuous local smoothing method are summarized in detail.

The local smoothing method for five-axis linear tool path must consider the constraints of approximation errors, synchronization and continuity. The approximation error bounds for the tool tip positions and tool orientations are evaluated with Eqs. (5) and (16), and the blending lengths and angle are constrained by Eqs. (6) and (18). The constraints of synchronization are defined by Eq. (9). Theorem 1 and Theorem 2 show the conditions for the constraint of C^2 continuity. As we can see, if the suitable blending lengths and angles are determined, all the constraints will be satisfied.

The main steps of the proposed local smoothing procedure are summarized in detail as follows.

Step I: Calculate the tool tip position blending l_ε and the tool orientation blending angle β_ε with the given error tolerances ε_{tip} and ε_{ori} using Eqs. (6) and (18).

Step II: Adjust the blending lengths and angle with Eq. (19) to achieve C^2 continuity:

$$\begin{aligned}\beta &= \min\left\{\beta_\varepsilon, \frac{3l_\varepsilon\phi}{4L_1}, \frac{3l_\varepsilon\psi}{4L_2}\right\}, \\ l_1 &= \frac{4L_1\beta}{3\phi}, \quad l_2 = \frac{4L_2\beta}{3\psi}.\end{aligned} \tag{19}$$

Step III: Calculate θ_i $(i = 0, \ldots, 7)$ with

$$\begin{aligned}\theta_2 &= \theta_3 = \theta_4 = \theta_5 \\ &= \frac{1}{2}\arcsin\left(\sin\beta\sqrt{\frac{\cos(\phi-\psi) - \mathbf{o}_0\cdot\mathbf{o}_2}{2\sin\phi\sin\psi}}\right), \\ \theta_0 &= \theta_1 = \theta_6 = \theta_7 = \frac{\beta}{2}.\end{aligned} \tag{20}$$

Step IV: Construct the control points of tool tip position with Fig. 1, and the control points of tool orientation with Fig. 2.

V. SIMULATION AND EXPERIMENTAL VALIDATION

To validate the feasibility of the proposed local path smoothing method, simulations and experiments are conducted on a TRT five-axis CNC machine tool with open

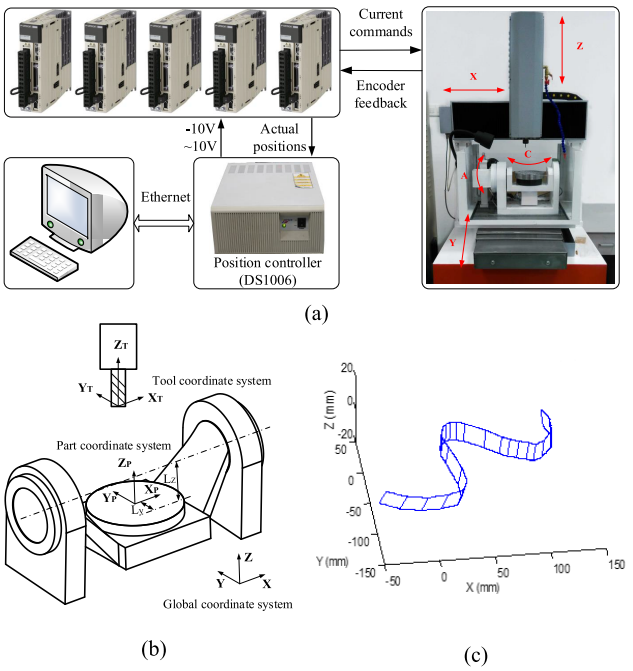

FIGURE 3. The experimental platform. (a) The layout of the experimental platform. (b) The kinematic configuration of the five-axis machine tool. (c) The experimental tool path.

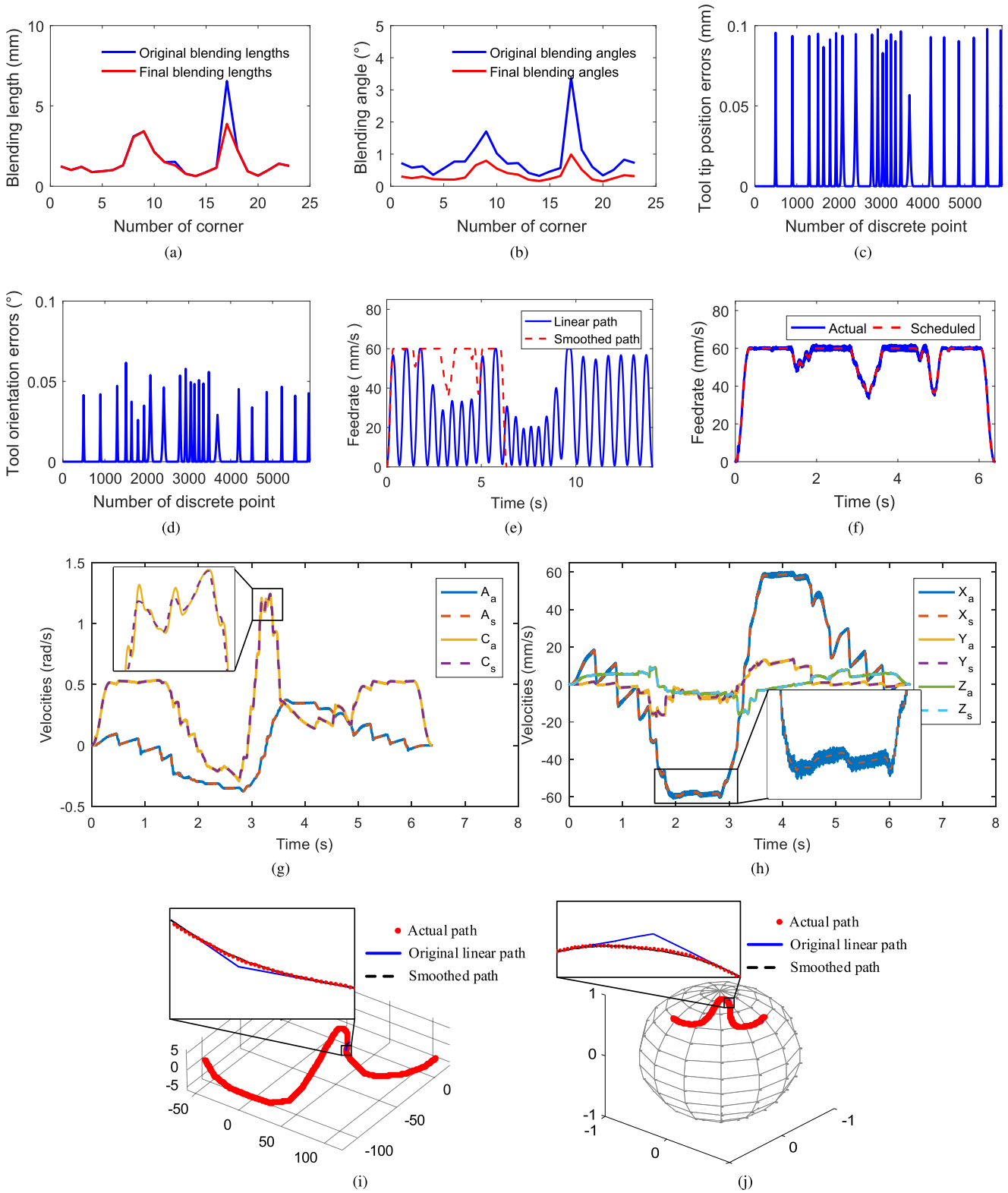

FIGURE 4. The simulation and experimental results. (a) Original and final blending lengths for tool tip position. (b) Original and final blending angles for tool orientation. (c) Tool tip position approximation errors. (d) Tool orientation approximation errors. (e) Feedrate comparison for the original linear tool path and the smoothed tool path. (f) Actual and original scheduled feedrate. (g) Actual and scheduled velocities of the rotary axes. (h) Actual and scheduled velocities of the translational axes. (i) Actual and original tool tip positions. (j) Actual and original tool orientations.

development environment. The layout of the system architecture for experiments is illustrated in Fig. 3 (a). The kinematic configuration of the CNC machine is shown in Fig. 3 (b). Given tool position $\mathbf{p} = [x, y, z]$ and tool orientation vector $\mathbf{o} = [i, j, k]$, the inverse kinematics transformation from part coordinate system to the machine coordinate system is

expressed as

$$\begin{cases} m_a = \arccos(k) \\ m_c = \arctan\frac{i}{j} \\ m_x = x\cos m_c + (L_y - y)\sin m_c \\ m_y = L_y + x\cos m_a \sin m_c \\ \quad + \left(y - L_y\right)\cos m_a \cos m_c + (L_z - z)\sin m_a, \\ m_z = L_z + x\sin m_a \sin m_c \\ \quad + \left(y - L_y\right)\sin m_a \cos m_c + (z - L_z)\cos m_a, \end{cases} \tag{21}$$

where m_a, m_c, m_x, m_y and m_z are the positions of the drive axes. The offsets of the rotary table are $L_y = 0$ *mm* and $L_z = 41$ *mm*, respectively. The machine tool is controlled by real-time controller dSPACE DS1006, and driven by YASKAWA SGDV series servo drivers and SGMJV motors. The standard PID controller is employed for each drive axis.

First, a five-axis linear tool path with 23 corners as shown in Fig. 3 (c) is smoothed with the proposed method. The simulation is conducted with MATLAB 2014b on a PC with Intel(R) Core(TM) i7-4770K 3.50 GHz CPU and 8 GB RAM. The tolerances for tool tip position ε_{tip} and tool orientation ε_{ori} are 0.1 mm and 0.1° respectively. The original blending lengths defined by the tolerances ε_{tip} and the final blending lengths $l = \max(l_1, l_2)$ are shown in Fig. 4 (a), the original blending angles defined by the tool orientation tolerance ε_{ori} and the final blending angles β are shown in Fig. 4 (b). We can find that, after the synchronization, the blending lengths and angles are adjusted. In this example, because the tolerance of tool tip position is stricter than that of tool orientation, the final blending angles are smaller than the original ones. The actual approximation errors are also provided in Fig. 4 (c) (d). As we can see, the actual errors of tool tip position and tool orientation are within the given tolerances. Unlike [22], the computations are all analytical. In this experiment, the total computational time for the path is 11 ms, and the average computational time for one corner is 0.48 ms. Therefore, the proposed method can be applied in real-time.

Second, the smoothed tool path is interpolated with the look-ahead method [14]. As a comparison, the original linear path is also interpolated. The resulting feedrate is shown in Fig. 4 (e). We can find that, the time elapsed is reduced from 14 s to 6.4 s, the efficiency is improved by 54.3%.

At last, the generated trajectory is send to the controller, and air-cutting experiments are conducted with the smoothed path on the five-axis CNC machine. The aim of this experiment is to test the tracking performance of the smoothed path by comparing the actual feedrate, velocities of each axis with the scheduled ones. The actual feedrate is shown in Fig. 4 (f), and the velocities of each axis are shown in Fig. 4 (g) (h), where the actual velocities are identified by subscript a, and the scheduled ones are identified by subscript s. We can find that, the actual velocities and feedrate have good agreement with the scheduled ones, which implies the smoothed path is easy to track for the controller. The actual tool tip positions and tool orientations are shown in Fig. 4 (i) (j), we can find the actual path nearly coincides with the smoothed path.

VI. CONCLUSION

In this paper, an analytical decoupled tool path local smoothing method for five-axis machining is proposed.

Compared with the existing works, the proposed method has the following advantages: (1) Tool orientation vector is smoothed with a pair of symmetric quartic spherical Bézier curves, which guarantees the unit property of tool orientation vector. (2) The C^2 continuity can be achieved with the synchronous path smoothing scheme. (3) The synchronous scheme and the approximation error bounds for both tool tip position and tool orientation are analytical; therefore, the proposed method can be employed in real-time.

Simulations and experiments are conducted on a TRT five-axis machine tool. The results demonstrate the efficiency and effectiveness of the proposed tool path local smoothing methodology.

APPENDIX A
PROOF OF EQ. (5)

Assuming $\mathbf{C}_e(u)$ is the transition B-spline with equal blending length l_1, and $\mathbf{C}_n(u)$ is the transition B-spline with unequal blending length, as shown in Fig. 5. By inserting knot $u = 0.5$ twice, $\mathbf{C}_e(u)$ can be transformed into two Bézier curves $\mathbf{B}_{e1}(u)$ and $\mathbf{B}_{e2}(u)$, which are defined by control points $\mathbf{Q}_{e0}$, $\mathbf{Q}_{e1}$, $\mathbf{Q}_{e2}$, $\mathbf{Q}_{e3}$ and $\mathbf{Q}_{e3}$, $\mathbf{Q}_{e4}$, $\mathbf{Q}_{e5}$, $\mathbf{Q}_{e6}$ respectively [22]. Similarly, $\mathbf{C}_n(u)$ can be transformed into two Bézier curves $\mathbf{B}_{n1}(u)$ and $\mathbf{B}_{n2}(u)$, which are defined by control points $\mathbf{Q}_{n0}$, $\mathbf{Q}_{n1}$, $\mathbf{Q}_{n2}$, $\mathbf{Q}_{n3}$ and $\mathbf{Q}_{n3}$, $\mathbf{Q}_{e4}$, $\mathbf{Q}_{e5}$, $\mathbf{Q}_{e6}$ respectively.

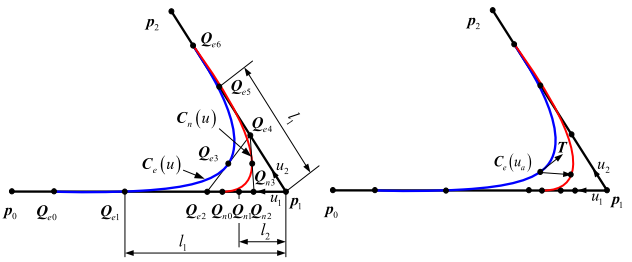

FIGURE 5. Analysis of the tool tip position approximation error.

The upper approximation error bound in Eq. (5) can be proved with the following two theorems:

Theorem 3: The approximation error of $\mathbf{C}_n(u)$ is smaller than the error of $\mathbf{C}_e(u)$.

Theorem 4: The maximum approximation error of $\mathbf{C}_e(u)$ is $l_1\cos(\theta/2)/2$.

A. PROOF OF THEOREM 3

Because three control points of $\mathbf{B}_{e1}(u)$ and $\mathbf{B}_{e2}(u)$ are collinear, with the variation diminishing property [22], it can be found that the Bézier curves do not wiggle, which implies that the transition B-spline $\mathbf{C}_e(u)$ is in the left side of its

tangent vector. Therefore, to prove Theorem 3, we only need to prove $\mathbf{C}_n(u)$ is in the right side of the tangent vector of $\mathbf{C}_e(u)$.

The control points of $\mathbf{B}_{e1}(u)$, $\mathbf{B}_{e2}(u)$, $\mathbf{B}_{n1}(u)$ and $\mathbf{B}_{n2}(u)$ are

$$\begin{aligned}
&\mathbf{Q}_{e0} = \mathbf{p}_1 + \frac{3}{2}l_1\mathbf{u}_1,\ \mathbf{Q}_{e1} = \mathbf{p}_1 + l_1\mathbf{u}_1,\\
&\mathbf{Q}_{e2} = \mathbf{p}_1 + \frac{1}{2}l_1\mathbf{u}_1, \mathbf{Q}_{e3} = \mathbf{p}_1 + \frac{\mathbf{u}_1+\mathbf{u}_2}{4}l_1,\\
&\mathbf{Q}_{e4} = \mathbf{p}_1 + \frac{1}{2}l_1\mathbf{u}_2,\ \mathbf{Q}_{e5} = \mathbf{p}_1 + l_1\mathbf{u}_1,\\
&\mathbf{Q}_{e6} = \mathbf{p}_1 + \frac{3}{2}l_1\mathbf{u}_1, \mathbf{Q}_{n0} = \mathbf{p}_1 + \frac{3}{2}l_2\mathbf{u}_1,\ \mathbf{Q}_{n1} = \mathbf{p}_1 + l_2\mathbf{u}_1,\\
&\mathbf{Q}_{n2} = \mathbf{p}_1 + \frac{1}{2}l_2\mathbf{u}_1,\ \mathbf{Q}_{n3} = \mathbf{p}_1 + \frac{l_2\mathbf{u}_1+l_1\mathbf{u}_2}{4}.
\end{aligned} \tag{22}$$

Then, the Bézier curves, the tangent vector $\mathbf{T}_1(u)$ of $\mathbf{B}_{e1}(u)$ and the tangent vector $\mathbf{T}_2(u)$ of $\mathbf{B}_{e2}(u)$ are expressed as

$$\begin{aligned}
\mathbf{B}_{e1}(u) &= \mathbf{p}_1 + \frac{3}{2}(1-u)^3 l_1\mathbf{u}_1 + 3u(1-u)^2 l_1\mathbf{u}_1\\
&\quad + \frac{3}{2}u^2(1-u)\,l_1\mathbf{u}_1 + u^3 l_1\frac{\mathbf{u}_1+\mathbf{u}_2}{4},\\
\mathbf{B}_{n1}(u) &= \mathbf{p}_1 + \frac{3}{2}(1-u)^3 l_2\mathbf{u}_1 + 3u(1-u)^3 l_2\mathbf{u}_1\\
&\quad + \frac{3}{2}u^2(1-u)\,l_2\mathbf{u}_1 + u^3\frac{l_2\mathbf{u}_1+l_1\mathbf{u}_2}{4},\\
\mathbf{B}_{e2}(u) &= \mathbf{p}_1 + (1-u)^3 l_1\frac{\mathbf{u}_1+\mathbf{u}_2}{4} + \frac{3}{2}u(1-u)^2 l_1\mathbf{u}_2\\
&\quad + 3u^2(1-u)\,l_1\mathbf{u}_2 + \frac{3}{2}u^3 l_1\mathbf{u}_2,\\
\mathbf{B}_{n2}(u) &= \mathbf{p}_1 + (1-u)^3\frac{l_2\mathbf{u}_1+l_1\mathbf{u}_2}{4} + \frac{3}{2}u(1-u)^2 l_1\mathbf{u}_2\\
&\quad + 3u^2(1-u)\,l_1\mathbf{u}_2 + \frac{3}{2}u^3 l_1\mathbf{u}_2,\\
\mathbf{T}_1(u) &= -\frac{3}{2}(1-u)^2 l_1\mathbf{u}_1 - 3u(1-u)\,l_1\mathbf{u}_1\\
&\quad + 3u^2 l_1\frac{\mathbf{u}_2-\mathbf{u}_1}{4},\\
\mathbf{T}_2(u) &= (1-u)^2 l_1\frac{\mathbf{u}_2-\mathbf{u}_1}{4} + 3u(1-u)\,l_1\mathbf{u}_2 + \frac{3}{2}u^2 l_1\mathbf{u}_2.
\end{aligned} \tag{23}$$

The Bézier curves $\mathbf{B}_{n1}(u)$ and $\mathbf{B}_{n2}(u)$ is in the right side of $\mathbf{T}_1(u)$ and $\mathbf{T}_2(u)$ for $u \in [0,\ 1]$ can be proved by

$$\begin{aligned}
&[\mathbf{B}_{n1}(u) - \mathbf{B}_{e1}(u)] \times \mathbf{T}_1(u)\\
&= \left[-\frac{3}{2}(1-u)^3 - 3u(1-u)^3 - \frac{3}{2}u^2(1-u) - \frac{1}{4}u^3\right]\Delta l\mathbf{u}_1\\
&\quad \times \left[\frac{15}{2}(1-u)^2 l_1\mathbf{u}_1 - 3u(1-u)\,l_1\mathbf{u}_1 + 3u^2 l_1\frac{\mathbf{u}_2-\mathbf{u}_1}{4}\right]\\
&= \left[\frac{3}{2}(1-u)^3 + 3u(1-u)^3 + \frac{3}{2}u^2(1-u) + \frac{1}{4}u^3\right]\\
&\quad \times \frac{3u^2 l_1\Delta l}{4}\sin\theta \geq 0,
\end{aligned}$$

$$\begin{aligned}
&[\mathbf{B}_{n2}(u) - \mathbf{B}_{e2}(u)] \times \mathbf{T}_2(u) = -(1-u)^3\Delta l\mathbf{u}_1\\
&\quad \times \left[(1-u)^2 l_1\frac{\mathbf{u}_2-\mathbf{u}_1}{4} + 3u(1-u)\,l_1\mathbf{u}_2 + \frac{3}{2}u^2 l_1\mathbf{u}_2\right]\\
&= (1-u)^3\left[(1-u)^2\frac{1}{4} + 3u(1-u) + \frac{3}{2}u^2\right]l_1\Delta l\sin\theta \geq 0.
\end{aligned} \tag{24}$$

where $\Delta l = l_1 - l_2 > 0$. □

B. PROOF OF THEOREM 4

Since $\mathbf{C}_e(u)$ can be transformed into two symmetrical Bézier curves $\mathbf{B}_{e1}(u)$ and $\mathbf{B}_{e2}(u)$, the approximation error is also symmetrical. The approximation error of $\mathbf{B}_{e1}(u)$ is analyzed here.

Because the linear segment $\mathbf{Q}_{e0}\mathbf{p}_1$ can be expressed as Bézier curve $\mathbf{L}(u)$ defined by the control points $\mathbf{Q}_{e0}$, $\mathbf{Q}_{e1}$, $\mathbf{Q}_{e2}$, $\mathbf{p}_1$. The deviation $\mathbf{L}(u)$ and $\mathbf{B}_{e1}(u)$ can be evaluated as

$$\varepsilon_t(u) = \|\mathbf{L}(u) - \mathbf{B}_{e1}(u)\| = u^3\|\mathbf{p}_1 - \mathbf{Q}_{e3}\| \tag{25}$$

Therefore, the maximum approximation error occurs at $u = 1$, and the maximum approximation error is

$$\varepsilon_{t\max} = \frac{l_1}{2}\cos\frac{\theta}{2}. \tag{26}$$

where θ is the angle of $\angle\mathbf{p}_0\mathbf{p}_1\mathbf{p}_2$. □

APPENDIX B
DERIVATIVES OF THE QUARTIC SPHERICAL BÉZIER CURVE AT TWO ENDS

For the quartic spherical Bézier curve of degree j, the first derivatives at $v = 0$ and $v = 1$ are

$$\begin{aligned}
\left.\frac{\mathrm{d}\mathbf{B}(v)}{\mathrm{d}v}\right|_{v=0} &= \frac{4\theta_0}{\sin\theta_0}(\mathbf{B}_1 - \mathbf{B}_0\cos\theta_0),\\
\theta_0 &= \arccos(\mathbf{B}_0\cdot\mathbf{B}_1),\\
\left.\frac{\mathrm{d}\mathbf{B}(v)}{\mathrm{d}v}\right|_{v=1} &= \frac{4\theta_3}{\sin\theta_3}(\mathbf{B}_4 - \mathbf{B}_3\cos\theta_3),\\
\theta_3 &= \arccos(\mathbf{B}_3\cdot\mathbf{B}_4).
\end{aligned} \tag{27}$$

The second derivatives at $v = 0$ and $v = 1$ are

$$\begin{aligned}
&\left.\frac{\mathrm{d}^2\mathbf{B}(v)}{\mathrm{d}v^2}\right|_{v=0}\\
&= -4\mathbf{B}_0{\theta_0}^2 + \frac{12\theta_0}{\sin^2\theta_0\sin\theta_1}\\
&\quad \times [\theta_1\sin\theta_0(\mathbf{B}_2 - \mathbf{B}_1\cos\theta_1) - \theta_0\cos\theta_0\sin\theta_1\\
&\quad \times (\mathbf{B}_1 - \mathbf{B}_0\cos\theta_0)]\\
&\quad - \frac{12}{\sin\theta_1\sin^3\theta_0}[\theta_0\sin\theta_0\sin\theta_1 + \theta_1\\
&\quad \times (\mathbf{B}_0\cdot\mathbf{B}_2 - \cos\theta_0\cos\theta_1)]\\
&\quad \times [\mathbf{B}_1(\sin\theta_0 - \theta_0\cos\theta_0) + \mathbf{B}_0(\theta_0 - \sin\theta_0\cos\theta_0)]
\end{aligned} \tag{28}$$

$$\begin{aligned}
&\left.\frac{\mathrm{d}^2\mathbf{B}(v)}{\mathrm{d}v^2}\right|_{v=1} \\
&= -4\mathbf{B}_4\theta_3^2 + \frac{12\theta_3}{\sin\theta_3} \\
&\quad\times\left[\frac{\theta_3\cos\theta_3}{\sin\theta_3}(\mathbf{B}_4\cos\theta_3 - \mathbf{B}_3) - \frac{\theta_2}{\sin\theta_2}\right. \\
&\quad\times(\mathbf{B}_3\cos\theta_2 - \mathbf{B}_2)] \\
&\quad-\frac{12}{\sin\theta_2\sin^3\theta_3}[\theta_3\sin\theta_2\sin\theta_3 + \theta_2 \\
&\quad\times(\mathbf{B}_2\cdot\mathbf{B}_4 - \cos\theta_2\cos\theta_3)\Big] \\
&\quad\times[\mathbf{B}_3(\sin\theta_3 - \theta_3\cos\theta_3) + \mathbf{B}_4(\theta_3 - \cos\theta_3\sin\theta_3)]\,.
\end{aligned} \tag{29}$$

REFERENCES

[1] *Manual 5-axis machining*, Siemens, 2009.
[2] *User's Manual HEIDENHAIN Conversational Programming*, Heidenhain, 2014.
[3] T. Otsuki and H. Shiobara, "5-axis machining features FANUC series 30i-model A/31i-model A5," *Fanuc Tech. Rev.*, vol. 19, pp. 1–6, Jan. 2006.
[4] S. S. Makhanov, "Adaptable geometric patterns for five-axis machining: A survey," *Int. J. Adv. Manuf. Technol.*, vol. 47, nos. 9–12, pp. 1167–1208, 2010.
[5] J. M. Langeron, E. Duc, C. Lartigue, and P. Bourdet, "A new format for 5-axis tool path computation, using Bspline curves," *Comput.-Aided Des.*, vol. 36, pp. 1219–1229, Oct. 2004.
[6] Y. Wang, X. Ma, L. Chen, and Z. Han, "Realization methodology of a 5-axis spline interpolator in an open CNC system," *Chin. J. Aeronaut.*, vol. 20, no. 4, pp. 362–369, 2007.
[7] W. Zhang, Y. F. Zhang, and Q. J. Ge, "Interference-free tool path generation for 5-axis sculptured surface machining using rational Bézier motions of a flat-end cutter," *Int. J. Prod. Res.*, vol. 43, no. 19, pp. 4103–4124, 2005.
[8] Q. Bi, Y. Wang, L. Zhu, and H. Ding, "An algorithm to generate compact dual NURBS tool path with equal distance for 5-axis NC machining," in *Proc. Int. Conf. Intell. Robot. Appl.* Berlin, Germany: Springer, 2010, pp 553–564.
[9] X. Zhao, H. Zhao, X. Li, and H. Ding, "Path smoothing for five-axis machine tools using dual quaternion approximation with dominant points," *Int. J. Precis. Eng. Manuf.*, vol. 18, no. 5, pp. 711–720, 2017.
[10] R. V. Fleisig and A. D. Spence, "A constant feed and reduced angular acceleration interpolation algorithm for multi-axis machining," *Comput.-Aided Des.*, vol. 33, pp. 1–15, Jan. 2001.
[11] A. Yuen, K. Zhang, and Y. Altintas, "Smooth trajectory generation for five-axis machine tools," *Int. J. Mach. Tools Manuf.*, vol. 71, pp. 11–19, Aug. 2013.
[12] J. Yang and Y. Altintas, "Generalized kinematics of five-axis serial machines with non-singular tool path generation," *Int. J. Mach. Tools Manuf.*, vol. 75, pp. 119–132, Dec. 2013.
[13] K. Yang and S. Sukkarieh, "An analytical continuous-curvature path-smoothing algorithm," *IEEE Trans. Robot.*, vol. 26, no. 3, pp. 561–568, Jun. 2010.
[14] H. Zhao, L. Zhu, and H. Ding, "A real-time look-ahead interpolation methodology with curvature-continuous B-spline transition scheme for CNC machining of short line segments," *Int. J. Mach. Tools Manuf.*, vol. 65, pp. 88–98, Feb. 2013.
[15] W. Fan, C.-H. Lee, and J.-H. Chen, "A realtime curvature-smooth interpolation scheme and motion planning for CNC machining of short line segments," *Int. J. Mach. Tools Manuf.*, vol. 96, pp. 27–46, Sep. 2015.
[16] M. Duan and C. Okwudire, "Minimum-time cornering for CNC machines using an optimal control method with NURBS parameterization," *Int. J. Adv. Manuf. Technol.*, vol. 85, pp. 1405–1418, Jul. 2015.
[17] X. Beudaert, P.-Y. Pechard, and C. Tournier, "5-Axis tool path smoothing based on drive constraints," *Int. J. Mach. Tools Manuf.*, vol. 51, pp. 958–965, Dec. 2011.
[18] Q. Bi, J. Shi, Y. Wang, L. Zhu, and H. Ding, "Analytical curvature-continuous dual-Bézier corner transition for five-axis linear tool path," *Int. J. Mach. Tools Manuf.*, vol. 91, pp. 96–108, Apr. 2015.
[19] X. Beudaert, S. Lavernhe, and C. Tournier, "5-axis local corner rounding of linear tool path discontinuities," *Int. J. Mach. Tools Manuf.*, vol. 73, pp. 9–16, Oct. 2013.
[20] Y. Jin, Q. Bi, and Y. Wang, "Dual-Bézier path smoothing and interpolation for five-axis linear tool path in workpiece coordinate system," *Adv. Mech. Eng.*, vol. 7, pp. 1–7, Jul. 2015.
[21] J. Shi, Q. Bi, L. Zhu, and Y. Wang, "Corner rounding of linear five-axis tool path by dual PH curves blending," *Int. J. Mach. Tools Manuf.*, vol. 88, pp. 223–236, Jan. 2015.
[22] S. Tulsyan and Y. Altintas, "Local toolpath smoothing for five-axis machine tools," *Int. J. Mach. Tools Manuf.*, vol. 96, pp. 15–26, Sep. 2015.
[23] J. Yang and A. Yuen, "An analytical local corner smoothing algorithm for five-axis CNC machining," *Int. J. Mach. Tools Manuf.*, vol. 123, pp. 22–35, Dec. 2017.
[24] L. A. Piegl, W. Tiller, *The NURBS Book*, 2nd. New York, NY, USA: Springer, 1997.
[25] T. A. Foley, D. A. Lane, G. M. Nielson, and R. Ramaraj, "Visualizing functions over a sphere," *IEEE Comput. Graph. Appl.*, vol. 10, no. 1, pp. 32–40, Jan. 1990.

XIN ZHAO received the B.E. degree from the School of Mechanical Science and Engineering, Huazhong University of Science and Technology, Wuhan, China, in 2013, where he is currently pursuing the Ph.D. degree. His research interests include CNC interpolation, motion planning, and robotic assembly.

HUAN ZHAO received the B.E. degree from the School of Mechanical Science and Engineering, Jilin University, Changchun, China, in 2006, and the Ph.D. degree from the School of Mechanical Engineering, Shanghai Jiao Tong University, Shanghai, China, in 2013. From 2013 to 2015, he was a Postdoctoral Researcher with the Huazhong University of Science and Technology, where he has been an Associate Professor, since 2015. His research interests include force control, visual servoing, and machine learning with applications to robotic machining.

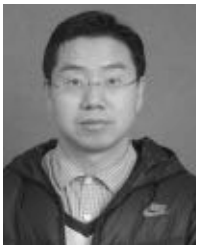

SHAOHUA WAN received the joint Ph.D. degree from the School of Computer, Wuhan University, and from the Department of Electrical Engineering and Computer Science, Northwestern University, USA, in 2010. Since 2015, he held a Postdoctoral position with the State Key Laboratory of Digital Manufacturing Equipment and Technology, Huazhong University of Science and Technology. From 2016 to 2017, he was a Visiting Scholar with the Department of Electrical and Computer Engineering, Technical University of Munich, Germany. He is currently an Associate Professor and the Master Advisor with the School of Information and Safety Engineering, Zhongnan University of Economics and Law. His main research interests include massive data computing for the Internet of Things and edge computing.

XIANGFEI LI received the B.E. degree from the School of Mechanical Science and Engineering, Jilin University, Changchun, China, in 2012. He is currently pursuing the Ph.D. degree with the Huazhong University of Science and Technology, Wuhan, China. His research interests include motion control and visual servoing.

HAN DING received the Ph.D. degree from the Huazhong University of Science and Technology, Wuhan, China, in 1989, where he has been a Professor, since 1997, and also the Director of the State Key Laboratory of Digital Manufacturing Equipment and Technology. Supported by the Alexander von Humboldt Foundation, he was with the University of Stuttgart, Germany, from 1993 to 1994. He was a Cheung Kong Chair Professor with Shanghai Jiao Tong University, from 2001 to 2006. His research interests include robotics, multi-axis machining, and control engineering. He was elected as the member of the Chinese Academy of Sciences, in 2013. He served as an Associate Editor for the IEEE TRANSACTIONS ON AUTOMATION SCIENCE AND ENGINEERING (TASE), from 2004 to 2007. He is currently an Editor of the IEEE TASE and a Senior Editor of the IEEE ROBOTICS AND AUTOMATION LETTERS.